OPEN BIOLOGY

royalsocietypublishing.org/journal/rsob

Research

Cite this article: Stamatiou K, Ligammari L, Bothota M, Tsavou A, Gokhan E, Cicirò Y, Zacarias M, Soucek L, Sala A, Vagnarelli P. 2026 A CDCA2–MYC positive feedback loop controls cancer cells survival. *Open Biol.* **16**: 250075.
https://doi.org/10.1098/rsob.250075

Received: 13 March 2025
Accepted: 20 January 2026

Subject Areas:
cellular biology, molecular biology

Keywords:
MYC, MYCN, protein phosphatase 1, CDCA2, neuroblastoma

Authors for correspondence:
Arturo Sala
e-mail: arturo.sala@brunel.ac.uk
Paola Vagnarelli
e-mail: paola.vagnarelli@brunel.ac.uk

Electronic supplementary material is available online at https://doi.org/10.6084/m9.figshare.c.8295614.

THE ROYAL SOCIETY PUBLISHING

A CDCA2–MYC positive feedback loop controls cancer cells survival

Konstantinos Stamatiou[1], Lorena Ligammari[1], Malki Bothota[1], Antonia Tsavou[1], Ezgi Gokhan[1], Ylenia Cicirò[1], Mariano Zacarias[2], Laura Soucek[3], Arturo Sala[1] and Paola Vagnarelli[1]

[1]Brunel University of London, London, UK
[2]Hospital University Vall d'Hebron Campus, Barcelona, Spain
[3]Institució Catalana de Recerca i Estudis Avançats, Barcelona, Spain

KS, 0000-0002-5650-078X; AS, 0000-0002-2841-7866; PV, 0000-0002-0000-2271

Cellular myelocytomatosis oncogene (MYC) transcription factors are encoded by a family of genes that include the prototype member *MYC*, *MYCN* and *MYCL*, and most human cancers display expression alterations of *MYC* genes. MYC is regulated at multiple levels, and its stability and activity are modulated by protein phosphorylation. Although there is a reasonable knowledge of the kinases required for MYC modifications, the counteracting phosphatases have been understudied. Here, we have investigated the role of the chromatin-associated protein phosphatase 1 (PP1) regulatory subunit CDCA2, also known as Repo-Man, in the regulation of MYC proteins in cancer cells. Using RNA interference and degron-mediated degradation of CDCA2, we have demonstrated that the PP1 subunit is required for cMYC and MYCN stabilization and viability of triple-negative breast cancer, neuroblastoma and colon cancer cells. Proximity ligation assays indicate that both cMYC and MYCN are in close proximity to CDCA2 *in vivo*. Furthermore, we have shown that *CDC2A* is a bona fide MYC target gene in cancer cells, revealing a reciprocal regulatory loop that could be exploited for therapeutic purposes.

1. Introduction

Cellular myelocytomatosis oncogene (MYC) is a transcription factor that regulates diverse cellular functions, including cell proliferation, apoptosis, pluripotency maintenance, cellular reprogramming and differentiation [1]. The MYC family encompasses the prototype member MYC (cMYC) and two other members, MYCN and MYCL, sharing a similar structure, including a transcription activation domain at the amino terminus and a basic Helix-Loop-Helix-leucine zipper (bHLHZ) domain at the carboxyl terminus involved in DNA binding [2]. The expression of *MYC* family genes is altered in the majority of human cancers, largely as a consequence of gene rearrangement or amplification, and is a driver of aggressive behaviour of tumour cells via target gene-dependent or independent transcription [3,4].

MYC proteins regulate gene transcription in association with MYC-associated factor X (MAX) [5]. The MYC–MAX heterodimer binds to E-box and non-E-box containing regulatory regions of 10–15% of all mammalian genes [6]. cMYC is also a short half-life protein (approx. 30 min) that is primarily regulated by the GSK3/SCF/FBXW7 pathway. Mitogen-regulated kinases phosphorylate cMYC at serine 62 (S62), and GSK3β then phosphorylates threonine 58 (T58), which triggers protein phosphatase 2A (PP2A)-mediated S62 dephosphorylation. This recruits the SCF-FBXW7 E3 ligase to direct cMYC ubiquitylation and subsequent proteasomal degradation [7].

However, cMYC can be phosphorylated at many other sites, and these phosphorylations are important for cMYC stability or function. Several kinases have already been identified as responsible for modifications of specific sites. For example, Aurora B kinase phosphorylates cMYC at serine 67 and promotes its protein stability [8], CDK2 can phosphorylate S62 and prevent Ras-induced senescence [9,10], while the stress response kinase Pak2 phosphorylates T358, S373 and T400 to reduce cMYC activity, as does phosphorylation by Protein kinase C zeta (PKCζ) at S373 [11].

The counteracting phosphatases for all these sites are so far unknown, but recent work suggested that protein phosphatase 1 (PP1) is a key phosphatase for cMYC, as inhibition of the catalytic subunit PP1c (or RNA interference (RNAi) of PP1c) leads to increased phosphorylation levels of several cMYC phosphosites [12].

PP1c in cells only exists in complex with other proteins that are regulatory interactors of protein phosphate 1 (RIPPOs). They target PP1 to substrates or modulate its catalytic activity, and more than 200 RIPPO/PP1 complexes have been identified so far. Therefore, searching for the relevant MYC–PP1 phosphatase complex is an important and challenging quest.

So far, only Phosphatase 1 Nuclear-Targeting Subunit (PNUTS)/PP1 has been identified as a cMYC phosphatase complex on chromatin [12,13], but the specificity for the sites still remains obscure. However, several other PP1/RIPPO complexes are known to modulate chromatin states and dynamics, and many have been associated with cancer. Here, we have discovered that another RIPPO, CDCA2 (also known as Repo-Man), interacts with MYC, and it is important for both cMYC and MYCN stability. We have also identified *CDCA2* expression as a very powerful prognostic marker for triple-negative breast cancer (TNBC) and *MYCN*-amplified neuroblastomas.

2. Results

2.1. *CDCA2* is co-expressed with *MYC* in triple-negative breast cancer and is essential for cancer cell survival

Although PP1 has been implicated in cMYC regulation, the mechanisms are not well understood. In several cell lines, PP1 inhibition by Caliculin A or PP1 knockdown significantly increased cMYC phosphorylation, leading to its degradation [12]. To understand the role of PP1 in MYC biology, it is important to identify the RIPPO(s) that mediate this function. Recent work has shown that PNUTS (PPP1R10) is one of the effectors of cMYC stability on chromatin [12–14].

However, considering the multiplicity of phosphosites within the cMYC protein [12] and the different types of chromatin it binds to (activator/repressor), it is plausible that multiple RIPPOs/PP1 complexes could be involved in its regulation at distinct types of chromatin [4].

We therefore conducted an initial screening using the University of California Santa Cruz (UCSC) cancer browser Xena (https://xena.ucsc.edu/welcome-to-ucsc-xena/) and the cancer genome atlas (TCGA) dataset for breast cancer to identify chromatin-associated RIPPOs linked to TNBC (a MYC-driven cancer) [15].

We selected NIPP1 (PPP1R8), PNUTS (PPP1R10), CDCA2 (PPP1R81), RIF1 and MKI-67, as all these RIPPOs have been associated with cancer before [12,13,16–26].

When comparing their mRNA levels with *MYC* expression, the analyses clearly highlighted a strong correlation for *PPP1R81 (CDCA2)* and *MYC*, even stronger than the one with *Ki-67*, a proliferation marker used in pathology to stage breast cancer [14]. CDCA2 is also known as Repo-Man, a chromatin-associated RIPPO important for cell division [21,27–33] (electronic supplementary material, figure S1A). *CDCA2* mRNA levels correlate with the stage of breast cancer (figure 1A), where higher expression is linked to more advanced stages, and they negatively impact the overall survival of breast cancer cases (figure 1B; datasets GSE42568) [34].

Interestingly, when stratified for cancer subtypes, *CDCA2* expression levels were significantly higher in TNBC (figure 1C and electronic supplementary material, figure S1A). The higher mRNA expression also correlates with higher protein levels in a TNBC cell line (HCC1143) and in the isogenic invasive MCF10A derivative Ca1H (also known to have high MYC levels [19]) compared to normal human mammary epithelial cells (HMEC) and the non-transformed MCF10A cells (figure 1D). Altogether, these data suggest a positive correlation between *MYC* expression and *CDCA2* that we sought to explore further.

We next investigated if CDCA2 was essential for cell survival in these cell types by a siRNA approach using the Ca1H cell line. We could successfully knockdown CDAC2 in the Ca1H cells (figure 1E), and the depletion caused cell death as shown by the increase of sub-G1 cells (electronic supplementary material, figure S1B) within 36 h. CDCA2 was also essential for wound closure in wound-healing assays (figure 1F) and negatively affected the proliferation/metabolism as evaluated in 3-(4,5-dimethylthiazol-2-yl)-2,5-diphenyltetrazolium bromide (MTT) assays (electronic supplementary material, figure S1C).

CDCA2 is a chromatin-bound protein. We previously mapped its preferred binding sites on HeLa cells' chromatin and showed that CDCA2 is important for the repression of several polycomb repressive complex 2 (PRC2)-regulated genes [27]. We therefore checked if *CDCA2*, which is overexpressed in TNBC, could also act as a repressor in this context. To this purpose, we analysed the gene expression profiles of the previously identified CDCA2-bound genes in normal mammary epithelium and TNBC samples using the UCSC cancer genomic platform. The analyses showed that the majority of CDCA2-bound genes negatively correlate with *CDCA2* expression in this cancer subtype and that the highest represented category belongs to the Genome Ontology (GO) terms of cell adhesion components (electronic supplementary material, figure S1D and table S1). Interestingly, 69.2% of them harbour a MYC-binding site at their promoter regions.

These analyses altogether let us conclude that CDCA2 is an important regulator of gene expression in TNBC and is essential for cell viability.

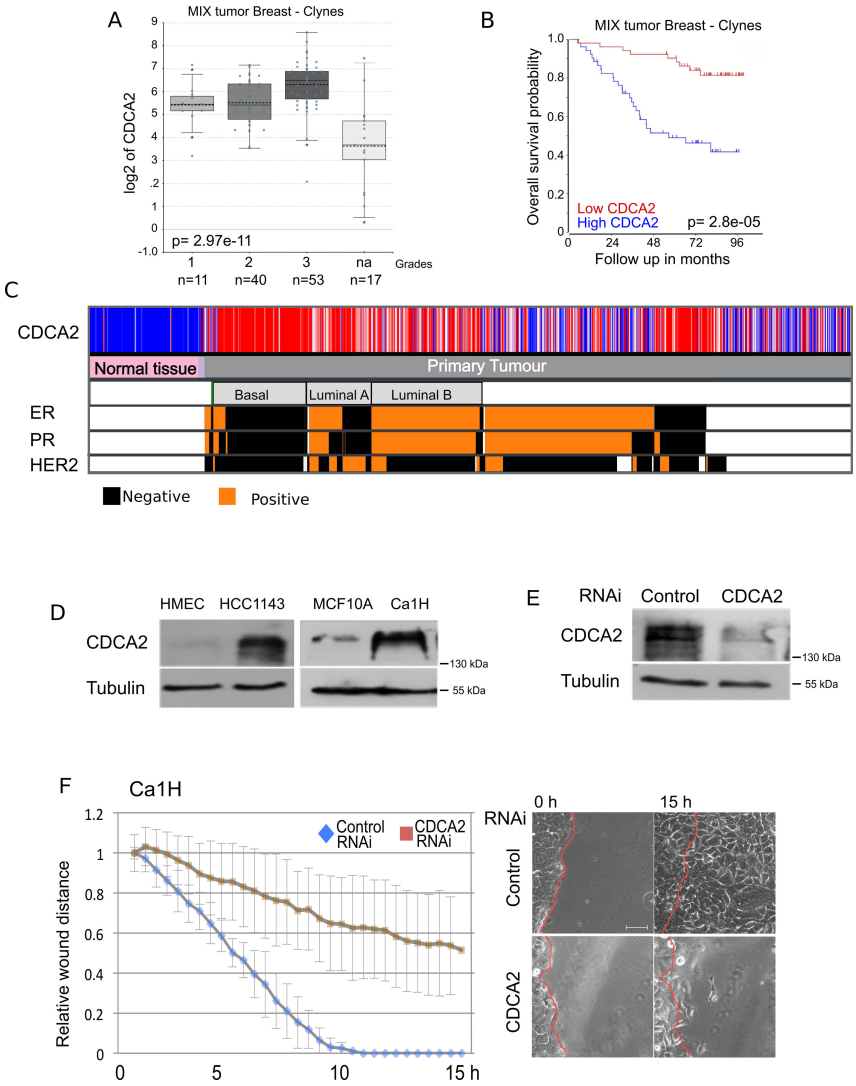

Figure 1. (A) *CDCA2* expression levels in mix breast tumours (Clynes dataset) of different grades. The graph was generated in the R2 genomic browser using the Clynes datasets (GSE42568) [34]. (B) Kaplan–Meier curve (survival probability in months) of breast tumour patients expressing low (red curve) or high (blue curve) levels of *CDCA2*. The graph was generated in the R2 genomic browser using the Clynes datasets (GSE42568) [34]. (C) UCSC cancer browser analyses of *CDCA2* expression levels (first row: blue, low expression; red, high expression) in breast cancer (primary tumour—grey) normal breast (normal tissue—pink; second row); the tumours were also stratified by type (third row: basal, luminal A and luminal B) and for oestrogen receptor (ER, fourth row), progesterone (PR, fifth row), Her 2 expression (sixth row) where orange indicates positivity and black negativity. (D) Western blot of HMEC, HCC1143, MCF10A and Ca1H cell lines. The blots were probed with anti-alpha tubulin and with anti-CDCA2 antibodies. (E) Representative western blot of Ca1H cell line transfected with control-Si or *CDCA2*-Si oligos for 36 h. The blot was probed with anti-alpha tubulin and with anti-CDCA2 antibodies. (F) Left: Quantification of relative wound distance of Ca1H cell line transfected with control Si (blue) or *CDCA2*-Si (orange) oligos. The values represent the average of three independent replicas, and the error bars are the s.d. The experiments were analysed by Student's *t*-test. ***$p < 0.001$. Right: Representative example of the experiment. Frames at the beginning of the experiment and at 15 h are shown. The red line indicated the boundary of the wound at time 0. Scale bar, 50 µm.

2.2. CDCA2 phosphatase activity and chromatin binding are essential for its function in triple-negative breast cancer

CDCA2 is a protein with several domains. These include (i) a region binding to PP1 and (ii) a binding site for chromatin (figure 2A). To test if these functions were necessary for wound healing in TNBC, we performed a set of rescue experiments with oligo-resistant green fluorescent protein (GFP)-tagged mutant forms of the protein in a *CDCA2* RNAi background. The experiments were conducted in the TNBC cell line HCC1143 where, similarly to what we obtained for the Ca1H cell line, *CDCA2* RNAi led to a defect in the closure of the wound (figure 2B). In these settings, while the GFP-tagged *wt* form of CDCA2 was able to rescue the wound closure defect caused by *CDCA2* RNAi, neither the chromatin binding mutant (GFP-CDCA2^{S893D}) [32,35] nor the one unable to bind PP1 (GFP-CDCA2^{RAXA}) [28] or GFP alone was able to do so (figure 2C–F). These experiments confirm that CDCA2 function in TNBC is PP1-dependent and requires binding to chromatin.

2.3. *CDCA2* is a MYC-regulated gene

Because of the strong correlation between *CDCA2* and c*MYC* expression in TNBC, we wondered if *CDCA2* could be itself a cMYC-regulated gene. Further inspection of the *CDCA2* promoter revealed the presence of three E-box MYC-binding sites [36],

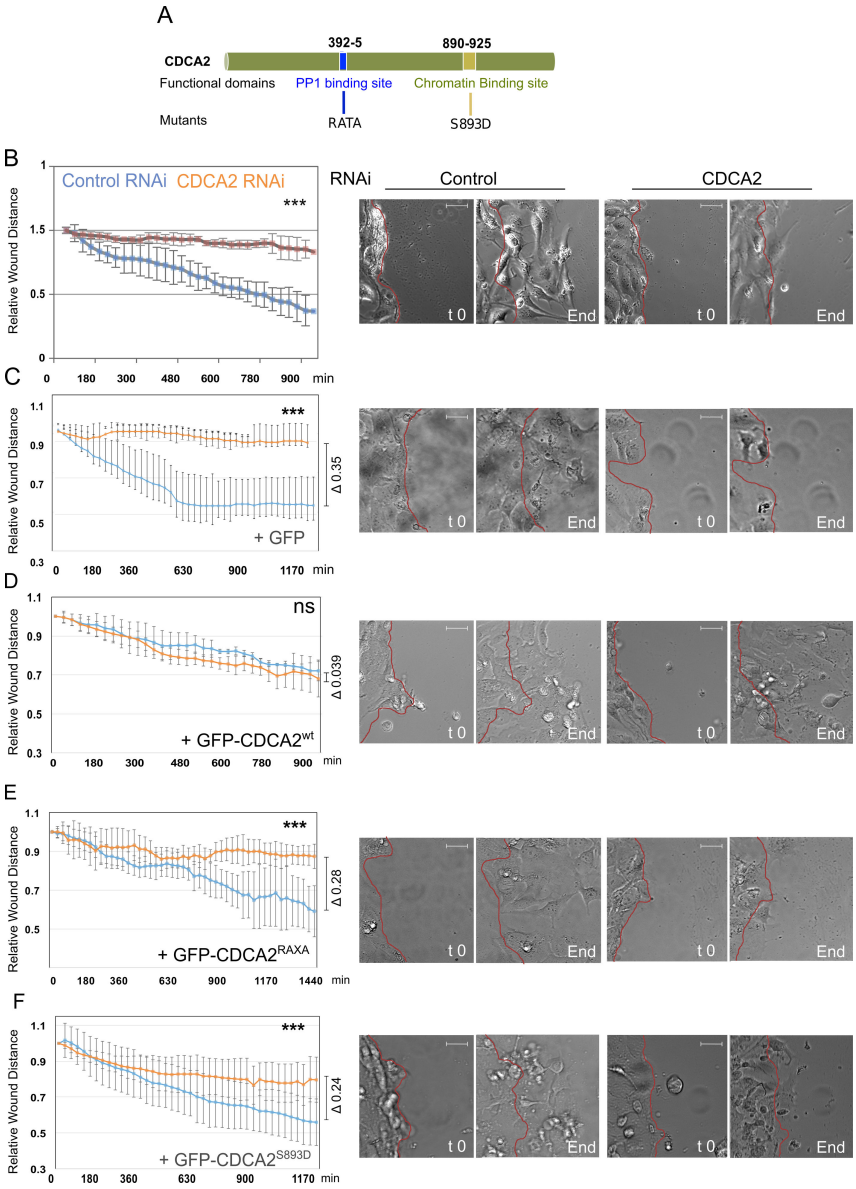

Figure 2. (A) Schematic of CDCA2 and its domains. RATA mutation at the PP1 binding site 392-6 and S893D mutation at the chromatin binding site 890-925 amino acids are highlighted in blue and light green, respectively. (B) Left: Quantification of the relative wound distance of HCC1143 cells transfected with control Si (blue) or *CDCA2*-Si (orange) oligos for 36 h. The values represent the average of three independent replicas, and the error bars are the s.d. The experiments were analysed by Student's *t*-test. ***$p < 0.001$. The Δ represents the difference between the control and *CDCA2*-Si at the end of the experiment. Right: Representative example of the experiment. Frames at the beginning of the experiment and at 15 h are shown. The red line indicated the boundary of the wound at time 0. Scale bars, 50 µm. (C–F) Quantification of relative wound distance of cells co-transfected with control Si (orange) or *CDCA2*-Si (blue) oligos and GFP (C), or oligo-resistant GFP-CDC2A^{wt} (D), GFP-CDC2A^{S893D} (E) and GFP-CDC2A^{RAXA} (F) plasmids for 36 h. The values represent the average of at least three independent replicas, and the error bars are the s.d. The experiments were analysed by Student's *t*-test. ns = not significant, ***$p < 0.001$.

and cMYC chromatin immunoprecipitation (ChIP) datasets showed in both MCF-7 and HeLa cells that MYC is present at the *CDCA2* promoter (figure 3A).

MYC inhibition can be achieved by a mini-protein called omomyc. Omomyc is a dominant-negative homologous to the bHLHZ of cMYC, containing point mutations that allow homodimerization and heterodimerization with MAX and all MYC family proteins [38]. Omomyc has been recently validated as an anticancer agent in patients with solid tumours in a Phase I trial [39]. Using this mini-protein inhibitor in the TNBC cell line MDA-MB231, *CDCA2* expression decreased by 2.9-fold (figure 3B), thus suggesting a link between cMYC and *CDCA2* expression.

As cMYC has also been linked to another RIPPO, PNUTS, whose promoter harbours MYC-binding sites as well (figure 3C), we checked if this PP1 interactor was also cMYC regulated. However, to our surprise, in this setting, Omomyc expression led to an increase in *PNUTS* mRNA of 1.4-fold, the opposite effect of *CDCA2* (figure 3B). This may suggest that cMYC acts more as a suppressor for PNUTS, at least in this cell type. Indeed, public TNBC datasets indicate that *PNUTS* (*PPP1R10*) expression is negatively correlated with that of MYC (electronic supplementary material, figure S1A—cnfPPP1R10 and MYC).

We then wanted to confirm that *CDCA2* was indeed a cMYC target. For this, we used a luciferase reporter assay where the *CDCA2* promoter containing the E-boxes was used to drive the expression of luciferase. Transfection of the *CDCA2*^{wt} promoter in the Ca1H cell line could drive the luciferase expression; however, when all the E-boxes of the *CDCA2* gene were mutated, the

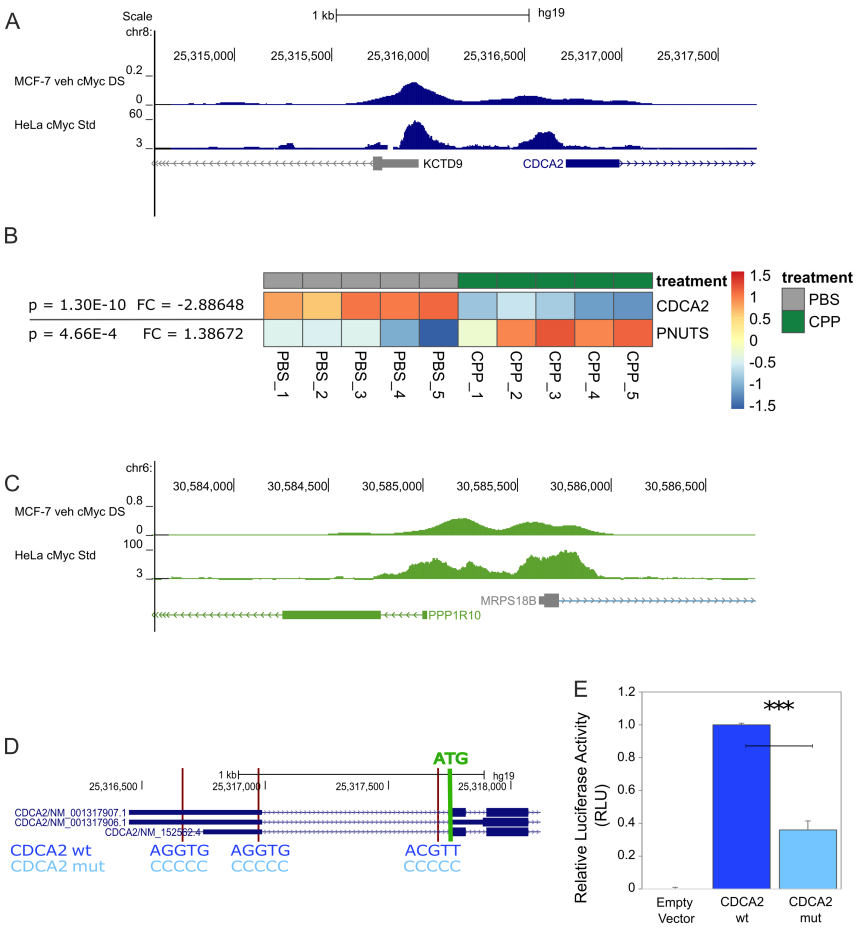

Figure 3. (A) cMYC chromatin immunoprecipitation sequencing profiles at the *CDCA2* locus in MCF-7 (GEO:GSM822301) and HeLa cell lines (GEO: GSM822286) [37]. (B) Microarray analysis of MDA-MB231 cells treated with 20 µM Omomyc (CPP) or PBS for 3 days. Values of *p*, fold change (FC) and heatmaps for CDCA2 and PNUTS. (C) cMYC chromatin immunoprecipitation sequencing profiles at the PNUTS (PPP1R10) locus in MCF-7 (GEO:GSM822301) and HeLa cell lines (GEO: GSM822286) [37]. (D) Schematic of the genomic locations selected to be mutated for the pGL3-CDCA2 wt/mut constructs used for the luciferase assay. The core MYC (AG/CGTG/T) binding sequence and the mutations introduced are indicated by the red lines at the promoter region of the *CDCA2* gene. (E) The bar plot indicates the relative light unit (RLU) values corrected for transfection efficiency with pRenilla luciferase. pGL3 empty vector was used to calculate the background luciferase activity. The values represent the average of three independent replicas and three technical replicas, and the error bars are the s.d. The experiments were analysed by Student's *t*-test. ns = not significant, ***$p < 0.001$.

promoter activity was significantly decreased (figure 3D,E). This clearly shows that *CDCA2* is a cMYC target gene and that it is essential for the proliferation of cMYC-driven breast cancer cells.

2.4. CDCA2 is required for cMYC stability

We then wondered how CDCA2 activity in TNBC was linked to cMYC biology. cMYC stability/degradation is regulated by phosphorylation, and the wound-healing experiments in breast cancer cells indicated that CDCA2 function is PP1-mediated. We therefore depleted CDCA2 in the Ca1H and the HCC1143 cell lines and quantified cMYC levels using immunofluorescence. The results clearly show that a significant decrease in cMYC levels was achieved upon CDCA2 depletion in both cell lines (figure 4A,B).

As RNAi could exert off-target effects (although we have shown that the wound healing can be rescued by GFP-CDCA2^{wt}), we took advantage of a more accurate system we recently developed to deplete CDCA2 using the endogenously tagged CDCA2 allele with an auxin degron module (AID), where the Oryza sativa Transport Inhibitor Response 1 (OsTR1) component is inducible by doxycycline (DOX). The addition of indole-3-acetic acid (IAA) to the system triggers the degradation of the specific protein, thus avoiding any possible off-target effect that the RNAi approach could cause (the validation of the cell line is in [40]). This cell line has been generated in HCT116, a colorectal cancer cell line in which cMYC expression is elevated and essential for survival [41].

Using this additional system, we could show that CDCA2 degradation leads to a decrease in cMYC protein levels (figure 4C,D). These data strengthen again the relationship between cMYC and CDCA2 and indicate that while cMYC is important for *CDCA2* expression, CDCA2 is also important for maintaining cMYC levels.

As previous work has linked the stability of cMYC protein levels to PNUTS [12], we wondered if the phenotype we observed was caused by an effect of CDCA2 on PNUTS. However, our analyses clearly show that CDCA2 degradation does not change PNUTS protein levels in HCT116 (figure 4C). To verify that the reported stabilization of cMYC by PNUTS was also occurring in HCT116 and was specific (previous data were only conducted by PP1 knockdown and inhibition), we used a similar cell line

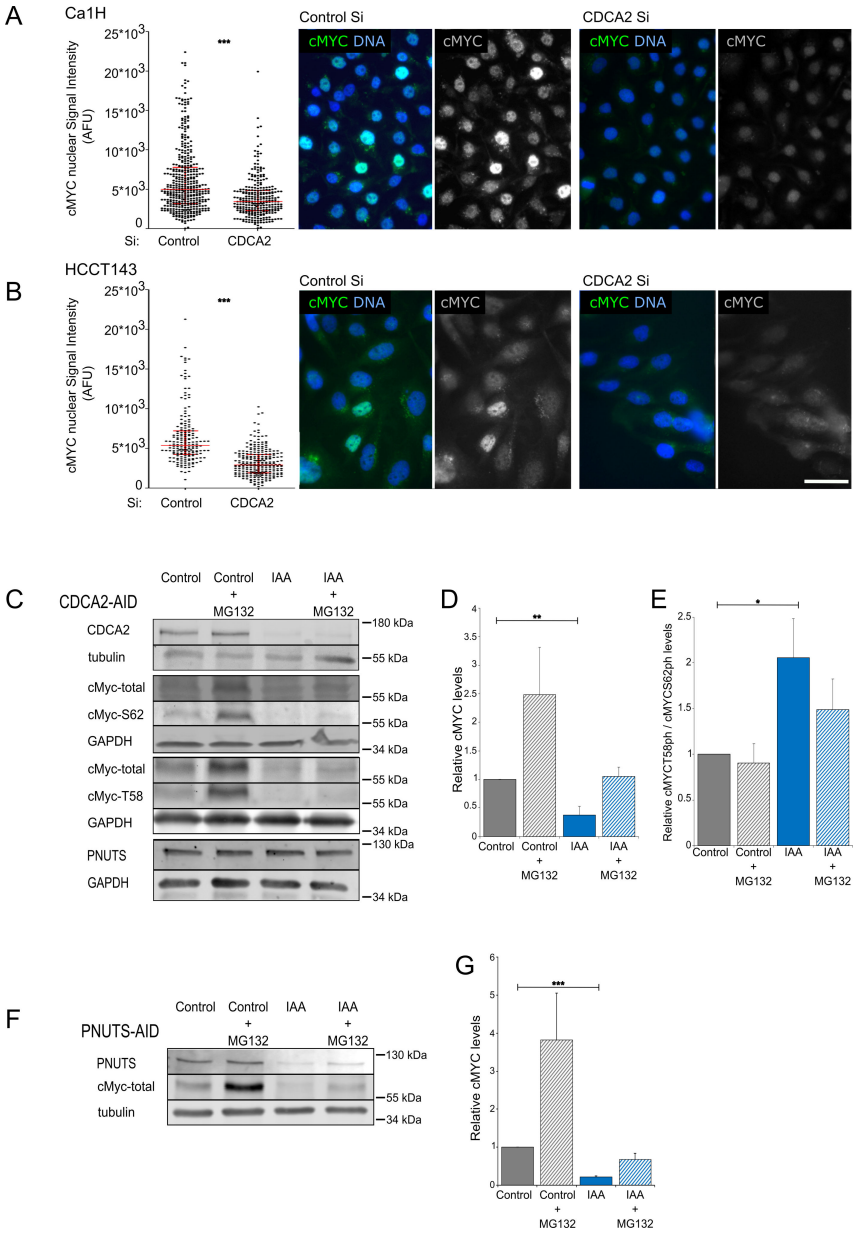

Figure 4. (A,B) Violin plot of the quantification of cMYC nuclear signal intensity (left). Whiskers are the upper and lower adjacent values, and the line is the median. A Wilcoxon test was conducted to compare the experiments. ***$p < 0.001$. Representative images (right) of the Ca1H (A) and HCC1143 (B) cell lines 48 h post-transfection with control or *CDCA2*-Si oligos, stained with cMYC antibodies (green) and counterstained with DAPI (blue). (C) Representative western blot of HCT116-CDCA2-AID cell line treated with doxycycline (DOX; 2 µg ml^{-1}) for 24 h before the addition of IAA, then untreated (Control) or treated with IAA (IAA) for 24 h followed by a 2 h treatment with 20 µM MG132 in the presence (IAA + MG132) or absence (Control + MG132) of IAA. The blots were probed with anti-GAPDH or anti-alpha tubulin antibodies and with anti-CDCA2, anti-PNUTS, anti-cMYC-total, anti-cMYC-S62ph and anti-cMYC-T58ph antibodies. The images were acquired with a LICOR Imaging system in the linear range for quantification purposes. (D) Quantification of total cMYC from the experiments in (C). The values represent the average of three independent replicas, and the error bars are the s.d. The experiments were analysed by Student's *t*-test. **$p < 0.01$. (E) Quantification of cMYC-T58ph/cMYC-S62ph from the experiments in (C). The values represent the average of three independent replicas, and the error bars are the s.d. The experiments were analysed by Student's *t*-test. *$p < 0.05$. (F) Representative western blot analyses of HCT116-PNUTS-AID cell line treated with DOX (2 µg ml^{-1}) 24 h before the addition of IAA, then untreated (Control) or treated with IAA (IAA) for 24 h followed by a 2 h treatment with 20 µM MG132 in the presence (IAA + MG132) or absence (Control + MG132) of IAA. The blots were probed with anti-alpha tubulin, anti-PNUTS and anti-cMYC-total antibodies. The images were acquired with a LICOR Imaging system in the linear range for quantification purposes. (G) Quantification of total cMYC from the experiments in (C). The values represent the average of three independent replicas, and the error bars are the s.d. The experiments were analysed by Student's *t*-test. ***$p < 0.001$.

where we have endogenously tagged PNUTS with the same degron module as CDCA2 [40]. Here, we could confirm that, upon addition of IAA and PNUTS degradation, cMYC protein levels decrease as previously reported (figure 4F,G) [12].

Overall, these data indicate that there are at least two RIPPOs involved in cMYC regulation.

As cMYC stability is regulated by its phosphorylation status, we investigated the levels of the T58ph and S62ph sites. The western blot analyses revealed that, upon CDCA2 degradation, the ratio between the T58ph and S62ph levels is increased in the presence of IAA, a signature that favours cMYC degradation (figure 4C,E).

The decrease in cMYC protein levels could be due to either increased degradation or arrest in G1 at the restriction checkpoint (therefore decreased *MYC* transcription), as caused by the depletion of CDCA2 or PNUTS. In fact, previous work in human squamous cell carcinoma cancer cells has shown a G1 arrest upon *CDCA2* SiRNA [42], and recent work from our laboratory has

highlighted a G1 block in cells where either CDCA2 or PNUTS was degraded in mitosis and then released [40]. We therefore set out to test these possibilities using the AID-tagged cell lines for PNUTS and CDCA2. In these experiments, we arrested the cells in thymidine (after the commitment stage and when *MYC* is already expressed), then we degraded the proteins for 4 h and analysed cMYC phosphorylation status and gene transcription levels.

At this cell-cycle stage, degradation of either CDCA2 or PNUTS leads to a decrease of cMYC protein levels and changes in the phosphorylation balance (electronic supplementary material, figure S2A–C,D–F). As previously seen for the asynchronous population, the ratio between cMYC T58ph/S62ph increases upon degradation of each protein, a signature for increased degradation. These experiments ruled out the hypothesis that the effect was the consequence of cell-cycle arrest in early G1.

CDCA2 depletion does not cause significant changes in either *CDCA2* or *PNUTS* mRNA. To further analyse the relationship between the two RIPPOs, we also investigated their relative protein levels in the degradation experiments. While CDCA2 degradation does not affect the protein levels of PNUTS (figure 4C), degradation of PNUTS affects CDCA2 protein levels (electronic supplementary material, figure S2G,H) but not its transcription (electronic supplementary material, figure S2I). However, either PNUTS or CDCA2 degradation decreases *MYC* expression in cells arrested with thymidine at the G1/S transition (electronic supplementary material, figure S2I–K). Interestingly, degradation of PNUTS increased its own transcription (electronic supplementary material, figure S2J).

These data altogether suggest that both RIPPOs are important for cMYC regulation and stability, and they seem to place PNUTS upstream of CDCA2, as degradation of PNUTS does affect CDCA2 levels.

Interestingly, we have also discovered a feedback loop in PNUTS regulation whereby its degradation leads to an increase in expression (electronic supplementary material, figure S2J).

2.5. *CDCA2* is regulated by MYCN in neuroblastoma and is essential for MYCN stability

Previous studies have shown that *CDCA2* is classified into a unique group of genes upregulated during the progression of neuroblastomas [43]. Since these tumours are often associated with *MYCN* amplifications, we wondered if *CDCA2* could also be linked to MYCN in this pathological condition.

We therefore first conducted *in silico* analyses of neuroblastoma gene expression datasets using the R2 genomic platform and interrogated the relationship between *MYCN* expression and the same set of chromatin-associated PP1 phosphatases used before for breast cancer. The analyses revealed that among all the RIPPOs investigated, *CDCA2* was the one where the expression levels were positively correlated with *MYCN* amplification and metastatic stage 4 (figure 5C,D), but also that expression of *CDCA2*, but not of other RIPPOs, was significantly associated with low patient survival (figure 5F and electronic supplementary material, figure S3A–C). This is in contrast with the expression levels of *PNUTS*, which have been previously linked to MYC regulation (figure 5A,B,E).

Based on these findings, and considering the knowledge we acquired on cMYC and CDCA2 regulation in TNBC and colon cancer cells, we wondered if a similar relationship between CDCA2 and MYCN also occurred in neuroblastoma.

We first tested whether MYCN was bound to the *CDCA2* promoter in neuroblastoma cell lines. Cystrome analyses of the MYCN ChIP-seq dataset revealed that MYCN was indeed present at the *CDCA2* promoter in both SHEP-21N (GEO GSM2113542) [45], which were engineered to conditionally express MYCN, and the naturally *MYCN*-amplified Kelly cell line (GEO GSM2113526) [45] (electronic supplementary material, figure S3D), suggesting that MYCN could be important for *CDCA2* transcription. To verify this, we used a cell line that does not express endogenous levels of *MYCN* but carries a MYCN transgene under the control of a DOX-repressible promoter [46]. Without DOX, *MYCN* is expressed, and the protein accumulates at high levels; upon addition of DOX, *MYCN* transcription is highly reduced after 24 h (figure 5G), and MYCN protein levels are negligible in the cells (figure 5H). The analyses of CDCA2 in these settings showed that, without DOX, *CDCA2* is highly expressed; however, upon addition of DOX, *CDCA2* mRNA expression decreases, as do its protein levels, with a lag time compared to MYCN (figure 5G,H); this is expected as CDCA2 requires the passage through mitosis to complete its degradation [47]. Furthermore, we analysed the levels of CDCA2 in a few MYCN-expressing cell lines and correlated their relative levels. The data showed that there is also a positive correlation between the levels of two proteins (electronic supplementary material, figure S3F,G).

Interestingly, *PNUTS* also shows accumulation of MYCN upstream of its transcription start site (TSS; electronic supplementary material, figure S3E), and repression of *MYCN* by addition of DOX in the SHEP-21 decreases PNUTS protein levels (figure 5I), although this does not seem to correlate with *MYCN* mRNA levels in neuroblastomas (figure 5A,B).

Altogether, these data indicate that also in neuroblastoma, *CDCA2* is a MYCN-regulated gene.

We therefore set out to investigate if MYCN stability in neuroblastoma was also linked to CDCA2 levels, as previously observed for MYC in breast cancer. We selected the *MYCN*-amplified LAN-1 and SK-N-B(2)-C and the SHEP-T21N cell lines. In these cells, we conducted *CDCA2* RNAi experiments and evaluated MYCN levels and its phosphorylation status. In all the cell lines, CDCA2 depletion is more difficult to obtain due to lower transfection efficiency, but even so, its reduction leads to a decrease in MYCN due to increased degradation (as addition of MG132 restores MYCN levels; electronic supplementary material, figure S4A,B,D,E,G,H). In addition, similar to what we observed for MYC, the T58ph/S62ph ratio was more elevated (electronic supplementary material, figure S4C,F,I), congruent with the observed MYCN degradation.

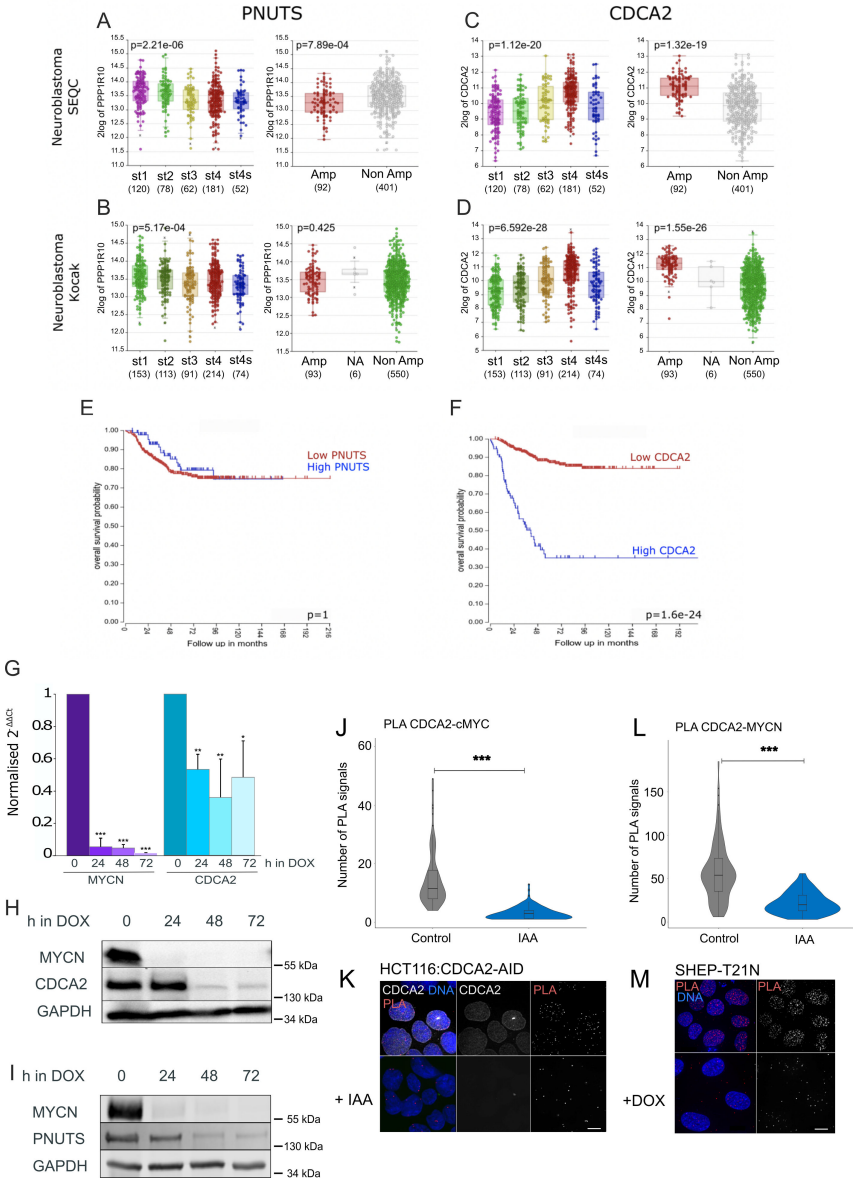

Figure 5. (A,B) *PNUTS* expression levels in neuroblastoma patients with different stages (st) of cancer (left) and *PNUTS* expression levels in neuroblastoma patients with (red) and without (grey) *MYCN* amplification (right) in the (A) SEQC cohort (GSE49710) and (B) Kocak cohort (GSE45547) [44]. The numbers indicate the sample sizes. (C,D) *CDCA2* expression levels in neuroblastoma patients with different stages (st) of cancer (left) and *CDCA2* expression levels in neuroblastoma patients with (red) and without (grey) *MYCN* amplification (right) in the (C) SEQC cohort (GSE49710) and (D) Kocak cohort (GSE45547). The numbers indicate the sample sizes. (E,F) Kaplan–Meier curve (survival probability in months) of neuroblastoma patients expressing low (red curve) or high (blue curve) levels of *PNUTS* (E) or *CDCA2* (F) Kocak cohort (GSE45547) [44]. (G) qPCR analyses of *MYCN* and *CDCA2* expression in SHEP-T21N treated without (0 h) or 1 µg ml^{-1} DOX for 24, 48 and 72 h. The data represent the average of three independent replicas, and the error bars are the s.d. The experiments were analysed by Student's *t*-test. *$p < 0.05$, ***$p < 0.001$. (H) Representative western blot analyses of SHEP-T21N treated without (0 h) or with 1 µg ml^{-1} DOX for 24, 48 and 72 h. The blots were probed with anti-alpha tubulin, anti-CDCA2 and anti-MYCN-total antibodies. (I) Representative western blot analyses of SHEP-T21N treated without (0 h) or with DOX for 24, 48 and 72 h. The blots were probed with anti-alpha tubulin, anti-PNUTS and anti-MYCN-total antibodies. (J) Quantification of the experiment in (K). The box inside the violin represents the 75th and 25th percentiles, whiskers are the upper and lower adjacent values and the line is the median. Sample size: control = 122, IAA = 126. A Wilcoxon test was conducted to compare the experiments and ***$p < 0.001$. (K) Representative images of the proximity ligation assay (PLA) using anti-cMYC and anti-GFP antibodies on HCT116:CDCA2-AID cell line with (top) or without (bottom) IAA. (L) Quantification of the experiment in (M). The box inside the violin represents the 75th and 25th percentiles, whiskers are the upper and lower adjacent values and the line is the median. Sample size: control = 179, IAA = 123. A Wilcoxon test was conducted to compare the experiments and ***$p < 0.001$. (M) Representative images of the PLA using anti-cMYC and anti-CDCA2 antibodies on SHEP-T21N cell line with (top) or without (bottom) DOX. Scale bar, 5 µm.

2.6. CDCA2 interacts with cMYC and MYCN

CDCA2 was previously identified as a cMYC-interacting protein in U2OS cells using an APEX-MYC proximity labelling approach [48] and also in HEK293T cells by a cMYC Bio-ID interactome, where it was shown to specifically interact with MYC homology boxes (MBs) MYC box IV (MBIV) [49].

However, these biochemical interactions have never been independently validated for cMYC, and no data are available for MYCN.

Because of the effect of CDCA2 depletion on cMYC and MYCN stability, we wanted to test if CDCA2 is indeed a bona fide cMYC or MYCN interactor in cells.

To this purpose, we conducted proximity ligation assays (PLAs) and tested the interactions between the endogenous CDCA2 and cMYC in the HCT116 cells and CDCA2 and MYCN in the TET-21 cell line. We could detect positive PLA signals confirming the interaction between CDCA2 and either cMYC or MYCN, which were significantly decreased either upon CDCA2 degradation by IAA (figure 5J,K) or MYCN repression by DOX (figure 5L,M).

3. Discussion

Despite decades of research, the regulation of cMYC stability and activity by post-translational modifications remains incompletely understood. Although cMYC is phosphorylated at numerous residues, only a subset of these modifications has been mechanistically linked to altered protein function or stability. Phosphatases, which counterbalance these phosphorylation events, have received far less attention than kinases. To date, PP2A is the best characterized phosphatase acting on cMYC, where dephosphorylation of S62 facilitates cMYC turnover [7].

A PP2A inhibitor, CIP2A, has been shown to be important for maintaining high cMYC S62 phosphorylation, critical for cMYC's ability to re-initiate proliferation and intestinal regeneration in response to DNA damage in mouse models. Interestingly, the major fraction of S62phMYC is bound to the nuclear envelope via CIP2A and selectively supports the stability of the lamina-associated pool of S62phMYC [50]. These observations underscore that the stability of MYC proteins is tightly linked to the balance between kinase and phosphatase activities and that disruption of this balance may also contribute to tumorigenesis.

Another phosphatase, PP1, has also been implicated in cMYC de-phosphorylation, but the only regulatory protein binding to PP1 (RIPPO) that has been characterized so far is PNUTS. PNUTS was identified in MYC-Bio-ID experiments, and it was shown that cMYC and PP1/PNUTS can coexist at promoters genome-wide. Inhibition or knockdown of PP1 leads to the hyperphosphorylation of cMYC and its dissociation from chromatin [12]. We and others have shown that PNUTS is a major regulator of transcription and that PNUTS degradation causes at least 2000 transcripts to be upregulated or downregulated [40]. PNUTS may control cMYC phosphorylation at these highly transcribed loci. Although PNUTS physically interacts with cMYC [13], PNUTS knockdown and rescue experiments have not been conducted so far. Moreover, it is not known if this link with cMYC is also valid for MYCN.

MYC can both activate and repress genes. For example, three genes encoding cell-cycle inhibitory proteins, *p15Ink4b*, *p21Cip1* and the *MYC*-antagonist *Mad4*, are repressed by cMYC through interaction with Miz-1 [51]. In addition, EZH2, the main enzymatic subunit of the PRC2, directly interacts with the MYC family oncoproteins cMYC and MYCN and promotes their stabilization by competing against the SCFFBW7 ubiquitin ligase to bind cMYC and MYCN [52]. Furthermore, direct recruitment of EZH2 by MYCN is associated with repressive chromatin marks at the promoter of bivalent genes and their silencing [53].

Our data demonstrate that CDCA2 depletion or targeted degradation destabilizes MYC proteins and enhances T58 phosphorylation, a key modification that promotes ubiquitin-mediated degradation (electronic supplementary material, figure S2A–D). Importantly, CDCA2 is enriched at H3K27me3-marked chromatin and bivalent promoters, in contrast to PNUTS, which is largely absent from repressed regions but sustains global transcription by promoting RNA polymerase II pause release [27]. This observation supports a model in which distinct PP1–RIPPO complexes exert site-specific control over MYC by anchoring phosphatase activity to particular chromatin contexts. Such compartmentalization could provide a mechanism for the cell to differentially regulate MYC's dual transcriptional functions—activation and repression—depending on chromatin state and promoter identity.

The discovery of a reciprocal regulatory loop, whereby MYC transcriptionally upregulates CDCA2, further underscores the oncogenic significance of this axis (figure 3). Positive feedback loops are a recurring theme in MYC biology and often serve to amplify oncogenic signals and stabilize malignant transcriptional programmes. The CDCA2–MYC loop adds to this repertoire by coupling post-translational stabilization of MYC with its transcriptional activity, thereby creating a self-reinforcing mechanism that promotes sustained oncogenic signalling. Given that CDCA2 expression correlates with poor prognosis in both TNBC and MYCN-amplified neuroblastoma, this feedback circuit likely represents a clinically relevant vulnerability (figure 1 and electronic supplementary material, figure S3).

From a translational standpoint, these findings highlight CDCA2 not only as a potential biomarker of MYC-driven tumours but also as a therapeutic target. Although direct pharmacological inhibition of MYC has proven challenging, targeting its cofactors and regulatory partners remains an attractive alternative. Modulating PP1 activity is difficult due to its widespread cellular functions, but the dependency of MYC-driven cancers on specific PP1–RIPPO complexes such as CDCA2 may allow for more selective therapeutic interventions. Strategies that disrupt the CDCA2–MYC interaction, destabilize CDCA2 or prevent its chromatin recruitment could represent novel avenues to impair oncogenic MYC function.

Nevertheless, several questions remain open. The exact phosphosites on cMYC and MYCN regulated by CDCA2–PP1 complexes remain to be identified, as does the extent to which this regulation overlaps or diverges from that mediated by PNUTS or other PP1 subunits. Furthermore, while our study demonstrates the functional importance of CDCA2 in cultured cells, validation in *in vivo* tumour models will be essential to determine the therapeutic tractability of this axis. Another open question is whether CDCA2 contributes to non-MYC-dependent functions relevant to tumorigenesis, given its role in chromatin regulation.

In conclusion, our study identifies CDCA2 as a critical regulator of cMYC and MYCN stability and establishes a CDCA2–MYC positive feedback loop that promotes cancer cell survival. This work broadens the understanding of how phosphatase

activity is spatially organized to regulate oncogenic transcription factors and suggests that selectively targeting PP1–RIPPO complexes could provide new opportunities for therapeutic intervention in MYC-driven malignancies.

4. Material and methods

MCF10A, MCF10A-TK1 and MCF10A-CA1h were obtained from the Karmanos Cancer Institute (via MTA) and maintained in DMEM/F12 (Invitrogen) supplemented with: 10% foetal bovine serum (FBS; Labtech), 1% penicillin–streptomycin (Gibco), 10 µg ml^{-1} insulin (Sigma), 20 µg ml^{-1} epidermal growth factor (EGF) (Perprotech), 0.5 µg ml^{-1} hydrocortisone (Sigma).

HCC1143 and SK-N-BE(2)-C cells were grown in Gibco RPMI 1640 GlutaMAX™ supplemented with 10% FBS (Labtech) and 1% penicillin–streptomycin (Gibco) at 37°C with 5% CO_2.

SHEP-T21N and LAN-1 cells were grown in Gibco DMEM GlutaMAX supplemented with 10% FBS (Labtech) and 1% penicillin–streptomycin (Gibco) at 37°C with 5% CO_2.

HCT116-CDCA2-AID and HCT116-PNUTS-AID cells were grown in Gibco™ McCoy's 5A Medium GlutaMAX supplemented with 10% FBS (Labtech) and 1% penicillin–streptomycin (Gibco) at 37°C with 5% CO_2.

4.1. Transfections

For siRNA treatments, HCC1143, Ca1H, SK-N-BE(2)-C, SHEP-T21N and LAN-1 cells were seeded into six-well plates, transfected using Polyplus JetPrime® (PEQLAB) with the appropriate siRNA oligonucleotides (50 nM) and analysed after 30–48 h. The siRNA oligos were published before [30] and obtained from Merck.

4.2. Immunofluorescence microscopy

Cells were fixed in 4% paraformaldehyde (PFA) and processed as previously described [29]. Primary and secondary antibodies were used as listed in table 1. Three-dimensional datasets were acquired using a wide-field microscope (NIKON Ti-E super research live cell imaging system) with a 100× Plan Apochromat lens, numerical aperture 1.45.

The datasets were deconvolved with the NIS Elements AR analysis software (NIKON). Three-dimensional datasets were converted to maximum projection, exported as TIFF files and imported into Inkscape for final presentation.

4.3. Immunoblotting

HCT116-CDCA2-AID and HCT116-PNUTS-AID cells were treated with DOX (2 µg ml^{-1}) and 2 mM thymidine, 24 and 18 h before the addition of IAA 1 mM, respectively. After the 4 h treatment with IAA, the cells were collected for protein extraction.

Whole-cell extracts were prepared by direct lysis in 1× Laemmli sample buffer [54].

Membranes were probed with the primary and secondary antibodies listed in electronic supplementary material, table S2, and visualized using either the Bio-Rad ChemiDoc XRS system or the LI-COR Odyssey imaging system, with images acquired in the linear range. For blots imaged with the LI-COR Odyssey, background signals were first subtracted from protein intensity values, and the resulting values were then normalized to the corresponding loading control. Because the LI-COR system measures fluorescence on a linear scale of light detection, quantification is more accurate and reliable compared to chemiluminescence-based systems. Treatment groups were compared with controls, and bar graphs represent data from at least three independent biological replicates. Statistical analyses were performed using a Student's *t*-test.

HMEC whole-cell lysates were provided by Prof. Newbold, Brunel University of London.

4.4. Flow cytometry cell-cycle analysis

Asynchronous cells, cells treated with 2 mM thymidine for 18 h, or HCT143 cells transfected with CDCA2 siRNA were trypsinized, resuspended and fixed in 70% ice-cold ethanol at room temperature for 30 min. Fixed cells were centrifuged at 1000*g* for 5 min, washed with PBS and the supernatant was discarded. The pellet was resuspended in 200 µl RNase A/PBS (100 µg ml^{-1}) and incubated at 37 °C for 2 h in the dark. Propidium iodide (Fisher Scientific, P3566) was added to a final concentration of 5 µg ml^{-1} immediately prior to analysis by flow cytometry using an ACEA Novocyte flow cytometer. Data were analysed with NovoExpress® software.

4.5. Proximity ligation assay

PLA was performed according to the manufacturer's protocol (Sigma). SHEP-T21N DOX (1 µg ml^{-1}) for 24 h and HCT116-CDCA2-AID cells were treated with DOX (2 µg ml^{-1}), 24 h before the addition of IAA (1000 µM) for 4 h. The cells were fixed, permeabilized and blocked with BSA as previously described [29].

Table 1. Summary of materials and resources used

reagent or resource	dilution	source	identifier
antibodies			
rabbit polyclonal CDCA2 rabbit	1:500(WB) 1:100(IF)	Abcam	catalogue no. AB45129 RRID:AB_869084
mouse monoclonal anti-MYCN (clone B8.4.B)	1:250(WB) 1:100(IF)	Santa Cruz Biotechnology	catalogue no. sc-53993 RRID:AB_831602
rabbit polyclonal anti-PNUTS	1:500(WB)	Thermo Fisher	catalogue no. PA5-61475 RRID:AB_2645848
mouse monoclonal anti-c-Myc (clone C-33)	1:200(WB) 1:100(IF)	Santa Cruz Biotechnology	catalogue no. Sc-42 RRID:AB_2282408
mouse monoclonal anti-α-tubulin (clone B-5-1-2)	1:10 000(WB)	Sigma-Aldrich	catalogue no. T5168 RRID:AB_477579
mouse monoclonal anti-GAPDH	1:10 000(WB)	Proteintech	catalogue no. 60004-1-Ig RRID:AB_2107436
goat polyclonal anti-rabbit HRP	1:10 000(WB)	Abcam	catalogue no. 31460
goat polyclonal anti-mouse HRP	1:10 000(WB)	Thermo Fisher Scientific	catalogue no. 31444 RRID:AB_228321
goat polyclonal anti-mouse 800CW	1:5000(WB)	LI-COR	catalogue no. 926-32210 RRID:AB_621842
goat polyclonal anti-rabbit 680RD	1:5000(WB)	LI-COR	catalogue no. 926-68071 RRID:AB_10956166
chemicals, peptides and recombinant proteins			
3-indoleacetic acid		Sigma-Aldrich	catalogue no. I2886 CAS:87-51-4
thymidine		Sigma-Aldrich	catalogue no. T9250 CAS:50-89-5
MG132		Millipore	catalogue no. 474787 CAS:133407-82-6
DOX		Sigma	catalogue no. D9891 CAS: 24390-14-5
oligonucleotides	siRNA sequence 5′–3′		
control	CGUACGCGGAAUACUUCGA[dT][dT]		
CDCA2	UGACAGACUUGACCAGAAATT		
critical commercial assays			
Duolink® In Situ PLA® Probe Anti-Rabbit MINUS	Sigma-Aldrich	catalogue no. DUO92005	
Duolink® In Situ PLA® Probe Anti-Mouse PLUS	Sigma-Aldrich	catalogue no. DUO92001	
Duolink® In Situ Detection Reagents Red	Sigma-Aldrich	catalogue no. DUO92008	
Luciferase Reporter Assay System	Promega	catalogue no. E1910	
MTT Cell Proliferation Assay Kit	Cayman Chemical	catalogue no. 10009365	

The antibodies were used at the following concentrations: 1 : 100 anti-CDCA2, 1 : 100 anti-MycN, 1 : 100 anti-cMyc and 1 : 10 000 anti-GFP [PABG1] (PABG1-20, RRID:AB_2749857). PLA probes were added, and ligation was performed following the manufacturer's instructions (Sigma). Coverslips were mounted and observed on the previously mentioned wide-field NIKON microscope.

4.6. MTT cell proliferation assay

Cells were seeded at a density of 5×10^3 per well in 96-well plates (triplicates) and transfected the following day with siRNA, oligo control or oligo targeting Repo-Man (50 nM) using JetPrime (Polyplus Transfection) according to the manufacturer's instructions. After 36 h of transfection, cell proliferation was assessed using an MTT Cell Proliferation Assay Kit (Cayman Chemical) following the manufacturer's protocol.

4.7. Wound-healing assay: live imaging and analysis

Cells (2×10^5 cells per well in 1 ml of medium) were grown overnight in a two-well chamber and transfected the following day with siRNA, oligo control or oligo against Repo-Man (50 nM) and 500 ng of GFP or GFP-CDC2A^{wt} or GFP-CDC2A^{S893D} or GFP-CDC2A^{RAXA} plasmid for 36 h. After 24 h, the medium in each chamber was replaced with Leibovitz's phenol-free medium, supplemented with antibiotics and serum. A wound was made in each well using a sterile tip, and the cells were transferred to a wide-field microscope (NIKON Ti-E super research live cell imaging system) at 37°C. Several points were chosen, and images were taken for the following 15–20 h every 30 min. At the final time point, Draq 5 (1 : 1000) was added to each chamber, and images were taken after 10 min. Nikon NIS Element software was used to analyse the assay. Briefly, the distance between the edges of the wound was measured at each time frame. The initial distance was used to normalize all the subsequent frames, and the values were used to generate the graphs.

4.8. Luciferase vectors construction and luciferase assay

To design the pGL3-CDCA2 wt plasmid, a 1367 bp region (CHR 8 25458872-25460239) of the CDCA2 promoter upstream of the TSS (codon ATG) was cloned into the pGL3-Basic backbone vector upstream of the luciferase gene. The pGL3-CDCA2 mut plasmid contains mutations of the canonical MYC-binding sequence present in the wt segment (figure 3D). Gene synthesis and cloning were performed by Biomatik Corporation.

For the luciferase assays, 5×10^4 per well of Ca1H cells were seeded in 24-well plates. The next day, cells were co-transfected with 0.25 µg of pGL3-CDCA2 (wt or mut) using JetPRIMER (Polyplus) and incubated for 36 h. pRenilla luciferase vector was used to control transfection efficiency. Luciferase activity was detected with a Dual-Luciferase Reporter Assay System (Promega).

4.9. Microarray analysis

MDA-MB-231 microarray analysis has been previously published [55]. Briefly, MDA-MB-231 cells were seeded and on the next day were treated with 20 µmol l^{-1} Omomyc or with an equivalent volume of vehicle. After 3 days, plates were washed twice with PBS and frozen at −80°C until processing. RNA was extracted with TRIzol reagent (Invitrogen) according to the manufacturer's instructions. The quality of RNA was confirmed with an Agilent 2100 Bioanalyzer. Clariom S Human HT microarray plate (Applied Biosystems) was processed at Vall d'Hebron Institute of Research (VHIR)'s High Technology Unit. The microarray data were analysed with Partek Genomics Suite software, v. 7.18. The expression heatmap was generated using R v. 4.4.1 in R Studio v. 2024.12.0+467, with the pheatmap package v. 1.0.12 (Kolde R (2018). pheatmap: Pretty Heatmaps. R package v. 1.0.12, https://github.com/raivokolde/pheatmap).

4.10. Quantitative polymerase chain reaction

The total RNA of HCT116-CDCA2-AID and HCT116-PNUTS-AID cells treated with 2 mM thymidine for 18 h (control and IAA treatment) was extracted using a Monarch Total RNA Miniprep Kit (New England Biolabs, Hitchin, UK), from which complementary DNA was synthesized by reverse transcription using RevertAid RT Reverse Transcription Kit (Thermo Fisher Scientific). qPCR was performed using Maxima SYBR Green/ROX qPCR Master Mix (2×; Thermo Fisher Scientific) using a QuantStudio 7 Flex Real-Time PCR Instrument (Thermo Fisher Scientific). The relative gene expression was calculated using the comparative Ct method (ΔΔCt). *GAPDH* was used as the endogenous reference gene.

qPCR was conducted using the following primers:
GAPDH Fw, 5′-ACCACAGTCCATGCCATCAC-3′;
GAPDH Rev, 5′-TCCACCACCCTGTTGCTGTA-3′;
CDCA2 Fw, 5′-GAGGCAGGAAAAGAGTCCGAGA-3′;
CDCA2 Rev, 5′- CTCCGACGTTTGGAGGACAACA-3′;
PNUTS Fw, 5′- CCCATAGACCCCAAAGAACTTC-3′;
PNUTS Rev, 5′-ATCGACTCACCATCTTTCGTG-3′;
cMyc Fw, 5′- AATGTCAAGAGGCGAACACAC-3′;
cMyc Rev, 5′- ATTGTTTTCCAACTCCGGAT-3′.

4.11. R2 genomics analyses

The Genomics Analysis and Visualization Platform (https://hgserver1.amc.nl/) was used to analyse the correlation of several RIPPO genes across neuroblastoma datasets Kocak and SEQC or the Clynes dataset for mix breast tumours and to generate the relative Kaplan–Meier plots.

4.12. Statistical analyses

Statistical analyses were performed using Microsoft Excel (Student's *t*-test) or R (Wilcoxon rank-sum test).

Ethics. This work did not require ethical approval from a human subject or animal welfare committee.

Data accessibility. The data underpinning the publication will be shared by the corresponding author upon request.

Electronic supplementary material is available online [56].

Declaration of AI use. We have not used AI-assisted technologies in creating this article.

Authors' contributions. K.S.: data curation, formal analysis, investigation, writing—review and editing; L.L.: data curation, formal analysis, investigation; M.B.: data curation, investigation; A.T.: formal analysis, investigation, writing—review and editing; E.G.: formal analysis, investigation, writing—review and editing; Y.C.: formal analysis, investigation; M.Z.: data curation, formal analysis, investigation, writing—review and editing; L.S.: data curation, formal analysis, investigation, writing—review and editing; A.S.: conceptualization, data curation, resources, supervision, validation, writing—original draft, writing—review and editing; P.V.: conceptualization, formal analysis, methodology, project administration, resources, supervision, visualization, writing—original draft, writing—review and editing.

All authors gave final approval for publication and agreed to be held accountable for the work performed therein.

Conflict of interest declaration. L.S. is co-founder, employee and shareholder of Peptomyc S.L. All the other authors do not have any competing interests.

Funding. The work on breast cancer was supported by a Breast Cancer Campaign PILOT grant to P.V. The work on neuroblastoma was supported by a KIDSCAN PhD studentship to P.V. and A.S. and a research grant from the Little Princess Trust to A.S. The results published here are in part based upon data generated by the TCGA Research Network: https://www.cancer.gov/tcga.

References

1. Zacarías-Fluck MF, Soucek L, Whitfield JR. 2024 MYC: there is more to it than cancer. *Front. Cell Dev. Biol*. **12**, 1342872. (doi:10.3389/fcell.2024.1342872)
2. Diolaiti D, McFerrin L, Carroll PA, Eisenman RN. 2015 Functional interactions among members of the MAX and MLX transcriptional network during oncogenesis. *Biochim. Biophys. Acta* **1849**, 484–500. (doi:10.1016/j.bbagrm.2014.05.016)
3. Baluapuri A, Wolf E, Eilers M. 2020 Target gene-independent functions of MYC oncoproteins. *Nat. Rev. Mol. Cell Biol*. **21**, 255–267. (doi:10.1038/s41580-020-0215-2)
4. Jakobsen ST, Siersbæk R. 2025 Transcriptional regulation by MYC: an emerging new model. *Oncogene* **44**, 1–7. (doi:10.1038/s41388-024-03174-2)
5. Sabò A, Amati B. 2014 Genome recognition by MYC. *Cold Spring Harb. Perspect. Med*. **4**, a014191. (doi:10.1101/cshperspect.a014191)
6. Eilers M, Eisenman RN. 2008 Myc's broad reach. *Genes Dev*. **22**, 2755–2766. (doi:10.1101/gad.1712408)
7. Boi D, Rubini E, Breccia S, Guarguaglini G, Paiardini A. 2023 When just one phosphate is one too many: the multifaceted interplay between Myc and kinases. *Int. J. Mol. Sci*. **24**, 4746. (doi:10.3390/ijms24054746)
8. Jiang J *et al*. 2020 Direct phosphorylation and stabilization of MYC by aurora B kinase promote T-cell leukemogenesis. *Cancer Cell* **37**, 200–215.(doi:10.1016/j.ccell.2020.01.001)
9. Hydbring P *et al*. 2010 Phosphorylation by Cdk2 is required for Myc to repress ras-induced senescence in cotransformation. *Proc. Natl Acad. Sci. USA* **107**, 58–63. (doi:10.1073/pnas.0900121106)
10. Hydbring P, Larsson LG. 2010 Tipping the balance: Cdk2 enables Myc to suppress senescence. *Cancer Res*. **70**, 6687–6691. (doi:10.1158/0008-5472.CAN-10-1383)
11. Kim JY *et al*. 2013 c-Myc phosphorylation by PKCzeta represses prostate tumorigenesis. *Proc. Natl Acad. Sci. USA* **110**, 6418–6423. (doi:10.1073/pnas.1221799110)
12. Dingar D *et al*. 2018 MYC dephosphorylation by the PP1/PNUTS phosphatase complex regulates chromatin binding and protein stability. *Nat. Commun*. **9**, 3502. (doi:10.1038/s41467-018-05660-0)
13. Wei Y *et al*. 2022 The MYC oncoprotein directly interacts with its chromatin cofactor PNUTS to recruit PP1 phosphatase. *Nucleic Acids Res*. **50**, 3505–3522. (doi:10.1093/nar/gkac138)
14. Finkelman BS, Zhang H, Hicks DG, Turner BM. 2023 The evolution of Ki-67 and breast carcinoma: past observations, present directions, and future considerations. *Cancers* **15**, 808. (doi:10.3390/cancers15030808)
15. Fallah Y, Brundage J, Allegakoen P, Shajahan-Haq AN. 2017 MYC-driven pathways in breast cancer subtypes. *Biomolecules* **7**, 53. (doi:10.3390/biom7030053)
16. Lashen AG, Toss MS, Ghannam SF, Makhlouf S, Green A, Mongan NP, Rakha E. 2023 Expression, assessment and significance of Ki67 expression in breast cancer: an update. *J. Clin. Pathol*. **76**, 357–364. (doi:10.1136/jcp-2022-208731)
17. Li W, Lv D, Yao J, Chen B, Liu H, Li W, Xu C, Li Z. 2023 A pan-cancer analysis reveals the diagnostic and prognostic role of CDCA2 in low-grade glioma. *PLoS One* **18**, e0291024. (doi:10.1371/journal.pone.0291024)
18. Sun W *et al*. 2023 CDCA2 promotes melanoma progression by inhibiting ubiquitin-mediated degradation of Aurora kinase A. *Eur. J. Cancer* **188**, 49–63. (doi:10.1016/j.ejca.2023.04.005)
19. Tang M, Liao M, Ai X, He G. 2021 Increased CDCA2 level was related to poor prognosis in hepatocellular carcinoma and associated with up-regulation of immune checkpoints. *Front. Med*. **8**, 773724. (doi:10.3389/fmed.2021.773724)
20. Gu P, Yang D, Zhu J, Zhang M, He X. 2022 Bioinformatics analysis of the clinical relevance of CDCA gene family in prostate cancer. *Medicine* **101**, e28788. (doi:10.1097/MD.0000000000028788)
21. Peng A, Lewellyn AL, Schiemann WP, Maller JL. 2010 Repo-man controls a protein phosphatase 1-dependent threshold for DNA damage checkpoint activation. *Curr. Biol*. **20**, 387–396. (doi:10.1016/j.cub.2010.01.020)
22. Egger JV, Lane MV, Antonucci LA, Dedi B, Krucher NA. 2016 Dephosphorylation of the retinoblastoma protein (Rb) inhibits cancer cell EMT via zeb. *Cancer Biol. Ther*. **17**, 1197–1205. (doi:10.1080/15384047.2016.1235668)
23. Marx A *et al*. 2020 Upregulation of phosphatase 1 nuclear-targeting subunit (PNUTS) is an independent predictor of poor prognosis in prostate cancer. *Dis. Markers* **2020**, 7050146. (doi:10.1155/2020/7050146)
24. Baxter JS *et al*. 2024 Cancer-associated FBXW7 loss is synthetic lethal with pharmacological targeting of CDC7. *Mol. Oncol*. **18**, 369–385. (doi:10.1002/1878-0261.13537)
25. Harvey-Jones E *et al*. 2024 Longitudinal profiling identifies co-occurring BRCA1/2 reversions, TP53BP1, RIF1 and PAXIP1 mutations in PARP inhibitor-resistant advanced breast cancer. *Ann. Oncol*. **35**, 364–380. (doi:10.1016/j.annonc.2024.01.003)
26. Zhou Y *et al*. 2024 MKI67 with arterial hypertension predict a poor survival for prostate cancer patients, a real-life investigation. *Clin. Transl. Oncol*. **26**, 3037–3049. (doi:10.1007/s12094-024-03505-5)
27. de Castro IJ *et al*. 2017 Repo-Man/PP1 regulates heterochromatin formation in interphase. *Nat. Commun*. **8**, 14048. (doi:10.1038/ncomms14048)
28. Trinkle-Mulcahy L, Andersen J, Lam YW, Moorhead G, Mann M, Lamond AI. 2006 Repo-Man recruits PP1 gamma to chromatin and is essential for cell viability. *J. Cell Biol*. **172**, 679–692. (doi:10.1083/jcb.200508154)

29. Vagnarelli P, Hudson DF, Ribeiro SA, Trinkle-Mulcahy L, Spence JM, Lai F, Farr CJ, Lamond AI, Earnshaw WC. 2006 Condensin and repo-man-PP1 co-operate in the regulation of chromosome architecture during mitosis. *Nat. Cell Biol*. **8**, 1133–1142. (doi:10.1038/ncb1475)
30. Vagnarelli P *et al*. 2011 Repo-Man coordinates chromosomal reorganization with nuclear envelope reassembly during mitotic exit. *Dev. Cell* **21**, 328–342. (doi:10.1016/j.devcel.2011.06.020)
31. Vagnarelli P. 2014 Repo-man at the intersection of chromatin remodelling, DNA repair, nuclear envelope organization, and cancer progression. *Adv. Exp. Med. Biol*. **773**, 401–414. (doi:10.1007/978-1-4899-8032-8_18)
32. Qian J, Beullens M, Lesage B, Bollen M. 2013 Aurora B defines its own chromosomal targeting by opposing the recruitment of the phosphatase scaffold repo-man. *Curr. Biol*. **23**, 1136–1143. (doi:10.1016/j.cub.2013.05.017)
33. Qian J, Lesage B, Beullens M, Van Eynde A, Bollen M. 2011 PP1/Repo-man dephosphorylates mitotic histone H3 at T3 and regulates chromosomal aurora B targeting. *Curr. Biol*. **21**, 766–773. (doi:10.1016/j.cub.2011.03.047)
34. Clarke C *et al*. 2013 Correlating transcriptional networks to breast cancer survival: a large-scale coexpression analysis. *Carcinogenesis* **34**, 2300–2308. (doi:10.1093/carcin/bgt208)
35. Huguet F, Gokhan E, Foster HA, Amin HA, Vagnarelli P. 2022 Repo-Man/protein phosphatase 1 SUMOylation mediates binding to lamin A and serine 22 dephosphorylation. *Open Biol*. **12**, 220017. (doi:10.1098/rsob.220017)
36. Gaubatz S, Meichle A, Eilers M. 1994 An E-box element localized in the first intron mediates regulation of the prothymosin alpha gene by c-myc. *Mol. Cell. Biol*. **14**, 3853–3862. (doi:10.1128/mcb.14.6.3853-3862.1994)
37. Zhang J *et al*. 2020 An integrative ENCODE resource for cancer genomics. *Nat. Commun*. **11**, 3696. (doi:10.1038/s41467-020-14743-w)
38. Massó-Vallés D, Soucek L. 2020 Blocking Myc to treat cancer: reflecting on two decades of omomyc. *Cells* **9**, 883. (doi:10.3390/cells9040883)
39. Garralda E *et al*. 2024 MYC targeting by OMO-103 in solid tumors: a phase 1 trial. *Nat. Med*. **30**, 762–771. (doi:10.1038/s41591-024-02805-1)
40. Stamatiou K, Huguet F, Budzinska M, deCastro IJ, Spanos C, Rappsilber J, Vagnarelli P. 2024 Multi-omic analyses reveal a differential contribution of chromatin-associated PP1 holoenzymes to mitotic exit and G1 re-establishment. *Bioarchive*. (doi:10.1101/2024.04.29.591626)
41. Lu JJ, Meng LH, Shankavaram UT, Zhu CH, Tong LJ, Chen G, Lin LP, Weinstein JN, Ding J. 2010 Dihydroartemisinin accelerates c-MYC oncoprotein degradation and induces apoptosis in c-MYC-overexpressing tumor cells. *Biochem. Pharmacol*. **80**, 22–30. (doi:10.1016/j.bcp.2010.02.016)
42. Uchida F, Uzawa K, Kasamatsu A, Takatori H, Sakamoto Y, Ogawara K, Shiiba M, Bukawa H, Tanzawa H. 2013 Overexpression of CDCA2 in human squamous cell carcinoma: correlation with prevention of G1 phase arrest and apoptosis. *PLoS One* **8**, e56381. (doi:10.1371/journal.pone.0056381)
43. Krasnoselsky AL, Whiteford CC, Wei JS, Bilke S, Westermann F, Chen QR, Khan J. 2005 Altered expression of cell cycle genes distinguishes aggressive neuroblastoma. *Oncogene* **24**, 1533–1541. (doi:10.1038/sj.onc.1208341)
44. Kocak H *et al*. 2013 Hox-C9 activates the intrinsic pathway of apoptosis and is associated with spontaneous regression in neuroblastoma. *Cell Death Dis*. **4**, e586. (doi:10.1038/cddis.2013.84)
45. Zeid R *et al*. 2018 Enhancer invasion shapes MYCN-dependent transcriptional amplification in neuroblastoma. *Nat. Genet*. **50**, 515–523. (doi:10.1038/s41588-018-0044-9)
46. Lutz W, Stöhr M, Schürmann J, Wenzel A, Löhr A, Schwab M. 1996 Conditional expression of N-myc in human neuroblastoma cells increases expression of alpha-prothymosin and ornithine decarboxylase and accelerates progression into S-phase early after mitogenic stimulation of quiescent cells. *Oncogene* **13**, 803–812.
47. Manzione MG, Rombouts J, Steklov M, Pasquali L, Sablina A, Gelens L, Qian J, Bollen M. 2020 Co-regulation of the antagonistic RepoMan:Aurora-B pair in proliferating cells. *Mol. Biol. Cell* **31**, 419–438. (doi:10.1091/mbc.e19-12-0698)
48. Solvie D *et al*. 2022 MYC multimers shield stalled replication forks from RNA polymerase. *Nature* **612**, 148–155. (doi:10.1038/s41586-022-05469-4)
49. Kalkat M *et al*. 2018 MYC protein interactome profiling reveals functionally distinct regions that cooperate to drive tumorigenesis. *Mol. Cell* **72**, 836–848.(doi:10.1016/j.molcel.2018.09.031)
50. Myant K *et al*. 2015 Serine 62-phosphorylated MYC associates with nuclear lamins and its regulation by CIP2A is essential for regenerative proliferation. *Cell Rep*. **12**, 1019–1031. (doi:10.1016/j.celrep.2015.07.003)
51. van de Wetering M *et al*. 2002 The beta-catenin/TCF-4 complex imposes a crypt progenitor phenotype on colorectal cancer cells. *Cell* **111**, 241–250. (doi:10.1016/s0092-8674(02)01014-0)
52. Wang L, Chen C, Song Z, Wang H, Ye M, Wang D, Kang W, Liu H, Qing G. 2022 EZH2 depletion potentiates MYC degradation inhibiting neuroblastoma and small cell carcinoma tumor formation. *Nat. Commun*. **13**, 12. (doi:10.1038/s41467-021-27609-6)
53. Corvetta D, Chayka O, Gherardi S, D'Acunto CW, Cantilena S, Valli E, Piotrowska I, Perini G, Sala A. 2013 Physical interaction between MYCN oncogene and polycomb repressive complex 2 (PRC2) in neuroblastoma: functional and therapeutic implications. *J. Biol. Chem*. **288**, 8332–8341. (doi:10.1074/jbc.M113.454280)
54. Laemmli UK. 1970 Cleavage of structural proteins during the assembly of the head of bacteriophage T4. *Nature* **227**, 680–685. (doi:10.1038/227680a0)
55. Massó-Vallés D *et al*. 2022 MYC inhibition halts metastatic breast cancer progression by blocking growth, invasion, and seeding. *Cancer Res. Commun*. **2**, 110–130. (doi:10.1158/2767-9764.CRC-21-0103)
56. Stamatiou K *et al*. 2026 Supplementary material from: A CDCA2 - MYC positive feedback loop controls cancer cells survival. Figshare. (doi:10.6084/m9.figshare.c.8295614)